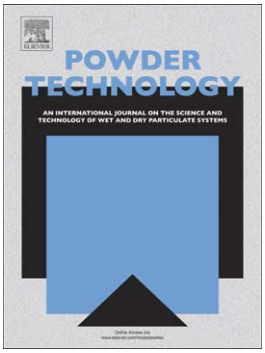

On the application of an Eulerian granular model towards dilute phase pneumatic conveying

J. Heng, T.H. New, W. Philip

PII: S0032-5910(17)31027-6
DOI: doi:10.1016/j.powtec.2017.12.069
Reference: PTEC 13058

To appear in: *Powder Technology*

Received date: 16 June 2017
Revised date: 18 December 2017
Accepted date: 22 December 2017

Please cite this article as: J. Heng, T.H. New, W. Philip, On the application of an Eulerian granular model towards dilute phase pneumatic conveying, *Powder Technology* (2017), doi:10.1016/j.powtec.2017.12.069

On the application of an Eulerian granular model towards dilute phase pneumatic conveying

J. Heng, T.H. New* and W. Philip

School of Mechanical and Aerospace Engineering, Nanyang Technological University
50 Nanyang Avenue, Singapore 639798

Abstract

The present study considered the application of a multiphase model with Eulerian approach for the solids phase in dilute-phase conveying, where the results are compared against previously published experimental results based on 42μm nominal diameter glass particles. In particular, the Favre-Averaged Drag turbulent dispersion model is studied where it is found to have greater effects on the particle concentration distribution as compared to the gas phase velocity. While certain discrepancies are observed between simulations and published experimental data, the flow characteristics are adequately captured after addressing the underlying cause of inaccuracies. Inaccuracies in the particle concentration distributions along a vertical pipe section result from the difficulty in capturing the transitional zone where the particle rope starts to disperse. On the other hand, particle diameter variations underpin the mismatches along a horizontal pipe section. Interestingly, increasing particle diameter leads to the successful capturing of the particle concentration distribution along the horizontal pipe section. The accuracy of employing an Eulerian approach for solids phase is demonstrated, provided that the particle diameter is accounted for.

Keywords: pneumatic conveying; two-phase flow, Eulerian granular model; numerical simulation

* Corresponding author: dthnew@ntu.edu.sg

1. Introduction

The use of pneumatic conveying systems to transport bulk materials over extended distances is commonplace for many industries. They had been utilized in power generation industry for the transport of pulverized coal; food industry for the transport of powdery ingredients such as wheat, flour or sugar; and construction industry for the transport of cement powder, to name a few. It stems from the many benefits that a pneumatic system provides over conventional belt conveying [1]. As the different industries continue to look for ways to improve their conveying systems, either for safety concerns or for increasing throughput, pneumatic conveying has been studied for many decades. Numerical simulations, or computational fluid dynamics (CFD), have emerged over the years as a reliable approach to study the mechanisms of pneumatic conveying. Investigations of dense or dilute flow regimes such as particle-laden flows, two-phase or multiphase flows, and moving bed flows, etc., are feasible through numerical simulations. Dense and dilute phase conveying are terms usually used to identify under which regime the flow is classified. Dense phase conveying generally encompass flows where the material is transported as a distinct phase from its carrier gas at the bottom of the channel whereas dilute flows generally mean that the particulates are entrained in the carrier gas phase. More detailed discussions on these flow classifications can be found in [1-4].

Due to their complexities, experimental studies are still being conducted to study pneumatic conveying processes. Some examples will include work by Khan et al. [5] on the pick-up velocity of particles and de Moraes et al. [6] on head loss coefficient for pipe fittings, both of which deal with properties fundamental to pneumatic conveying processes. While experimental studies form a significant portion of pneumatic conveying investigations, the number of numerical simulation studies are increasing as well. Over the years, many

researchers had come up with many different models catering to different conditions or areas of interest in the flow. Apart from direct numerical simulations (DNS) and solving the complete equations of motion for each individual particle, there is no one unified model to use for a gas-particle flow in which current computers can handle. In most cases, only the most appropriate modelling is being applied for certain cases to reduce computational cost. These include the selection of either an Eulerian or Lagrangian approach of the solids phase based on the flow regime [7], a two-way or four-way coupling between the phases depending on the particle loading ratio [8], Stokes number [9], and various turbulent models, although some models have consistently shown more accuracy over other models. Descriptions of these numerical models will be presented in greater detail in Section 2.

The most commonly investigated aspect within pneumatic conveying is the pressure drop within the pipes. McGlinchey et al. [10] used the Eulerian formulation and predicted pressure drops in 90° bends. Their results demonstrated qualitative agreement with experimental data. In another case, Makwana et al. [11] looked into the effects of dune formation on pressure drops. Dunes, formed at the bottom of the pipe during some conveying processes, were found numerically to induce large pressure fluctuations. In other aspects, Li et al. [12] predicted solid deposition characteristics using the Lagrangian formulation. As the Lagrangian model was used, only fairly large particles were modelled within their computations. Nevertheless, the study was able to shed light on the interaction of particles. They described how a particle plug would interact with the layer of deposited material left by the previous plug, and how the plug leaves some material behind as it traverses along the pipe. Hidayat and Rasmuson [13] investigated the gas-solid flow characteristics within a U-bend in attempt to optimize a pneumatic conveying dryer system. They detailed the effects of the bend radius on the distribution of particles and the gas velocity and further concluded the importance of these two parameters on the efficiency of the dryer. Other applications include investigation of plug

flows in step-up pipe arrangements [14], of very fine powders [15], of bend orientations [16] and of a combination of two bends [17]. Such investigations demonstrated the practical applications of numerical simulations in the understanding pneumatic conveying flow characteristics in different situations.

Consequently, there was a demand for more accuracy in numerical simulation models. As researchers work towards developing a more robust and accurate numerical model to study particle-laden flows, most of them have turned towards using a Lagrangian particle treatment for dilute flows [18]. One of the reasons for solving the complete equations of motion for the particles is to obtain highly accurate simulations of particle-laden flows. However, the primary downside of the Lagrangian model is that with current computing architectures, it is simply not feasible to scale up the computations to study real-life industrial applications due to computational costs [19]. For studies with more complex geometry or higher solids loading ratio, the Eulerian scheme remains the only practical approach in terms of computational cost and time. However, one of the concerns surrounding the Eulerian scheme is its assumption of a continuum. This means that the actual dynamics of the flow starts to deviate from the assumptions as the particle phase gets more dilute, i.e. the distance between particles increases [2]. Van Deemter and van der Laan [20] performed the pioneering work of deriving the balance equations by integration methods. Anderson and Jackson [21] later on used the equations of motion for a particle, together with the Navier-Stokes equations for fluid motion, and came up with the set of governing equations that is still used today in many commercial computing software. However, many constitutive relations could not be obtained directly by their method. A large part of this initial gap has since been filled with models either derived with another method or by empirical correlations. These include, for example, the interface drag term [22-24], granular temperature [25] and solid shear stresses [26].

One of the closure relations that should be highlighted here is the turbulent dispersion model. Because the distribution of particles (even in areas with relatively low particle concentrations) has been shown to affect the flow structures of the gas phase [27-29], it is essential to accurately model the particle distributions. Turbulent dispersion is the mechanism for the particle phase to be transported from regions of high concentration to lower concentrations [30] and this is especially so after a pipe bend. Burns et al. [30] utilized Favre averaging of the interphase drag term to obtain the additional terms in the momentum equations that account for turbulent dispersion. The authors had named it the Favre Averaged Drag model. This model finds itself most commonly used in scenarios pertaining to gas-liquid flows (i.e. droplets or bubbly flows). Of the currently known publications that either referred to or utilized the Favre Averaged Drag (FAD) model in their numerical models, none had applications dealing with gas-solid dilute phase flows. This is despite the original authors concluding that the model is a generalization of other turbulent dispersion models and it should hold true for a wide range of multi-phase flow scenarios. Furthermore, to the best knowledge of the present authors, there were no known restrictions raised in the existing literature in terms of applying this particular turbulent dispersion model towards a dilute gas-solid flow.

This study primarily aims to demonstrate the ability of an Eulerian scheme in predicting the flow characteristics of a granular phase in a pneumatic pipe configuration featuring a 90° bend. Both the upstream and downstream portions of the pipe bend will be studied, with a focus on the particle distribution, as well as both the gas and particle velocities. As detailed above, the application of the FAD model towards a gas-solid multiphase flow remains scarce in the literature. Here, the authors intend to document the effects of the FAD model on a flow where one of the phases is a granular phase. Specifically, the empirical model constant will be varied to observe its effects and to select a suitable constant. The objective is to investigate

if this model possesses the ability to be extended to gas-solid dilute flows. Lastly, the effects of the particle diameter used within the model will also be briefly touched upon.

2. Numerical model

The Eulerian scheme (also known as the Eulerian-Eulerian scheme in some cases) treats both the gas and solid phases separately. It incorporates a set of conservation equations for each phase and is interpenetrating. The gas is treated as the usual fluid phase by the numerical model. For the solid phase, the solid was treated as a continuum akin to the gas phase and is only differentiated by designating it as a granular phase. A granular phase has additional parameters and constitutive relations that are required to fully model the phase. One advantage of the Eulerian granular model is that it can be used for comparatively large computational domains with proportionally more solid particles. As opposed to the Lagrangian method where the equation of motion is solved for each and every particle within the system, the Eulerian granular model solves only one conservation equation for each defined solid phase. Therefore, the Eulerian granular model scales in complexity only with the domain size and not the number of particles. The Eulerian granular model applies kinetic theory to the solid particles to derive the conservation equation. Hence, it trades off a little accuracy for calculation speed. If the Lagrangian method were to be applied to a large domain with proportionally more solid particles, the number of equations solved also increases proportionally. Therefore, a Lagrangian formulation on the current study was not possible with the computing resources available. The Eulerian granular model treats the secondary phase (i.e. cement, in this case) as a continuous ‘fluid’ and interactions between particles themselves can be formulated with kinetic theory. The decision of closure relations most suitable to the flow is made following recommendations presented in the literature. Most notably, van Wachem et al. [31] performed a comprehensive comparison between

different governing equations and closure relations within the Eulerian granular model which set a basis for the appropriate modelling to apply in this study.

2.1 Governing equations

Fluent (ANSYS, Inc) 13.0 was used for the current study. The conservation equations follow the work of Anderson and Jackson [21]. Navier-Stokes equations for a fluid and Newton's equation of motion for a single particle were used to derive the following conservation equations.

The mass conservation for phase q is:

$$\frac{\partial}{\partial t}\left(\alpha_q \rho_q\right) + \nabla \cdot \left(\alpha_q \rho_q \overrightarrow{v_q}\right) = 0 \tag{1}$$

The momentum conservation equation is:

$$\frac{\partial}{\partial t}\left(\alpha_q \rho_q \overrightarrow{v_q}\right) + \nabla \cdot \left(\alpha_q \rho_q \overrightarrow{v_q}\overrightarrow{v_q}\right) = -\alpha_q \nabla p + \nabla \cdot \bar{\bar{\tau}}_q + \alpha_q \rho_q \vec{g} + \sum_{p=1}^{n} \vec{R}_{pq} + \vec{F}_{td,q} \tag{2}$$

where $\bar{\bar{\tau}}_q$ in equation (2) is the q^{th} phase stress-strain tensor:

$$\bar{\bar{\tau}}_q = \alpha_q \mu_q \left(\nabla \vec{v}_q + \nabla \vec{v}_q^T\right) + \alpha_q \left(\lambda_q - \frac{2}{3}\mu_q\right) \nabla \cdot \vec{v}_q \bar{\bar{I}} \tag{3}$$

The interphase interaction term $\vec{R}_{pq}$ in equation (2) is:

$$\sum_{p=1}^{n} \vec{R}_{pq} = \sum_{p=1}^{n} K_{pq}\left(\vec{v}_p - \vec{v}_q\right) \tag{4}$$

where K_{pq} is the interphase momentum exchange coefficient and is a combination of the Ergun [22] model at solid volume fractions larger than or equal to 0.2 and the Wen and Yu [23] model at solid volume fractions lower than 0.2. Ergun's model was determined by the pressure drop of an experiment for fixed liquid-solid beds at packed conditions whereas Wen and Yu's model was correlated from solid particle settling experiments over a wide range of

volume fractions. In this study, only the gas-solid drag is included. The gas-solid exchange coefficient K_{pq} in equation (4) (here K_{sg} for easier distinction between gas and solid phase) is:

$$K_{sg} = \frac{3}{4} C_D \frac{\alpha_s \alpha_g \rho_g \left|\vec{v}_s - \vec{v}_g\right|}{d_s} \alpha_g^{-2.65} \tag{5}$$

when $\alpha_g > 0.8$ and

$$C_D = \frac{24}{\alpha_g Re_s}\left[1 + 0.15\left(\alpha_g Re_s\right)^{0.687}\right] \tag{6}$$

with d_s being the particle diameter and Re_s being the relative Reynolds number:

$$Re_s = \frac{\rho_g d_s \left|\vec{v}_s - \vec{v}_g\right|}{\mu_g} \tag{7}$$

For when $\alpha_g \leq 0.8$,

$$K_{sg} = 150 \frac{\alpha_s\left(1-\alpha_g\right)\mu_g}{\alpha_g d_s^2} + 1.75 \frac{\rho_g \alpha_s \left|\vec{v}_s - \vec{v}_g\right|}{d_s} \tag{8}$$

The different formulation for different gas volume fraction as in equations (5-8) follows the suggestion of Gidaspow [24]. The turbulent dispersion force $\vec{F}_{td,q}$ in equation (2) is modelled with the FAD model [30] that is included in the software, according to equations (9-10) below. It was developed by time averaging the conservation equations that were derived by ensemble averaging. For the solid phase, $\vec{F}_{td,s}$ is:

$$\vec{F}_{td,s} = C_{TD} K_{gs} \frac{D_s}{\sigma_{gs}} \left(\frac{\nabla \alpha_g}{\alpha_g} - \frac{\nabla \alpha_s}{\alpha_s}\right) \tag{9}$$

where the dispersion scalar D_s is:

$$D_s = \frac{\mu_{ts}}{\rho_s} \tag{10}$$

For the momentum conservation equation of the solids phase shown in equation (2), there will be an additional solids pressure term $(+\nabla p_s)$ on the right-hand side. This term is analogous to the pressure of the gas phase as the solids phase equations is derived following

kinetic theory. However, unlike the gas phase pressure which takes a quantifiable value, the solids pressure has to be modelled further and it represents the solid phase forces due to the particle-particle interactions. The solids pressure follows the work of Lun et al. [26] and it takes the form of:

$$p_s = \alpha_s \rho_s \Theta_s + 2\rho_s(1+e_{ss})\alpha_s^2 g_{0,ss}\Theta_s \tag{11}$$

As with the fluid pressure having its solids pressure counterpart, the fluid temperature has the corresponding granular temperature term. The transport equation for granular temperature derived by Ding and Gidaspow [25] is:

$$\begin{aligned} &\frac{3}{2}\left[\frac{\partial}{\partial t}(\rho_s \alpha_s \Theta_s) + \nabla\cdot(\rho_s \alpha_s \vec{v}_s \Theta_s)\right] \\ &\qquad = \left(-p_s\bar{\bar{I}} + \bar{\bar{\tau}}_s\right):\nabla\vec{v}_s + \nabla\cdot\left(k_{\Theta_s}\nabla\Theta_s\right) - \gamma_{\Theta_s} + \phi_{gs} \end{aligned} \tag{12}$$

where the diffusion coefficient k_{Θ_s} is provided by Syamlal et al. [32] who neglected the kinetic contribution from the expression by Lun et al. [26], because it tends to an unphysical value at low volume fractions:

$$k_{\Theta_s} = \frac{15 d_s \rho_s \alpha_s \sqrt{\Theta_s \pi}}{4(41-33\eta)}\left[1 + \frac{12}{5}\eta(4\eta-3)\alpha_s g_{0,ss} + \frac{16}{15\pi}(41-33\eta)\eta\alpha_s g_{0,ss}\right] \tag{13}$$

with $\eta = 0.5(1+e_{ss})$ and the collisional dissipation of energy γ_{Θ_s} is that of the expression by Lun et al. [26] based on the assumption of slight inelasticity:

$$\gamma_{\Theta_s} = \frac{12(1-e_{ss}^2)g_{0,ss}}{d_s\sqrt{\pi}}\rho_s \alpha_s^2 \Theta_s^{\frac{3}{2}} \tag{14}$$

and $\phi_{gs} = -3K_{gs}\Theta_s$ is the energy exchange between the phases. Equations (13-14) closes the granular transport equation (12) and the granular temperature solution can be used to determine the solids shear viscosity. The radial distribution function $g_{0,ss}$ is:

$$g_{0,ss} = \left[1 - \left(\frac{\alpha_s}{\alpha_{s,max}}\right)^{\frac{1}{3}}\right]^{-1} \tag{15}$$

The solids shear viscosity μ_s can be written as consisting of three parts, collisional, kinetic and frictional part where the collisional part following Lun et al. [26] is:

$$\mu_{s,col} = \frac{4}{5}\alpha_s \rho_s d_s g_{0,ss}(1+e_{ss})\left(\frac{\Theta_s}{\pi}\right)^{\frac{1}{2}}\alpha_s \tag{16}$$

the kinetic part following Gidaspow et al. [33] is:

$$\mu_{s,kin} = \frac{10\rho_s d_s\sqrt{\Theta_s \pi}}{96\alpha_s(1+e_{ss})g_{0,ss}}\left[1+\frac{4}{5}g_{0,ss}\alpha_s(1+e_{ss})\right]^2\alpha_s \tag{17}$$

and the frictional part following Johnson and Jackson [34] is:

$$\mu_{s,fr} = 0.1\alpha_s \frac{\left(\alpha_s - \alpha_{s,min}\right)^2}{\left(\alpha_{s,max} - \alpha_s\right)^5}\sin\phi \tag{18}$$

where ϕ is the internal angle of friction. Equations (16-18) are then summed to get the total solids shear viscosity. The bulk viscosity λ_s (λ_q in equation 3) is modelled by Lun et al. [26] as:

$$\lambda_s = \frac{4}{3}\alpha_s^2 \rho_s d_s g_{0,ss}(1+e_{ss})\left(\frac{\Theta_s}{\pi}\right)^{\frac{1}{2}} \tag{19}$$

With equation (19) and the standard $k-\epsilon$ turbulence model used for the gas phase turbulence, the set of equations is closed. For the Eulerian granular model, a 'per-phase' turbulence modelling was applied, where a set of separate $k-\epsilon$ turbulence equations was solved for each phase.

2.2 Problem description and boundary conditions

The current numerical simulation problem was based on a previous experimental work performed by Huber and Sommerfeld [35], where detailed descriptions of the experimental setup could be found. Experimental results provided by them will be used to compare against numerical simulation results arising from the present study. In their experimental study, spherical glass beads were conveyed by air through a pipe bend. The diameter of the glass

beads was sampled by phase doppler anemometry and found to vary as a skewed distribution within the range $0\mu m < d < 100\mu m$. However, the particle diameter was set to a particle size of $42\mu m$ in the current numerical simulations, following the number mean diameter the original authors had documented to allow more direct comparisons. By affixing the particle diameter to take a single value, it reduced numerical complexities by not having to define more than one solid phase. The material density was defined as $2500kg/m^3$. The pipe diameter was set to $0.08m$, similar to that used by the experimental study, and consisted of a 90° horizontal-to-vertical bend. The length of the straight pipe section before and after the bend was $5.5m$ and $3m$ respectively.

A mass flow rate inlet boundary condition was applied to match the original experiments; in which they had controlled the amount of material introduced into the pipe by screw feeders. The outlet boundary condition was set to a pressure outlet to atmospheric pressure. At the walls, different treatment was applied for both of the phases. A no-slip condition was applied for the gas phase and a specularity coefficient of 0.6 was applied for the solid phase. The specularity coefficient is used for a rough wall and it defines the collision characteristics of a particle with the wall, with a value of 0 being a perfectly smooth wall. For a wall roughness height that is comparable to the particle diameter, the specularity coefficient will be large [36]. However, this value is not easily determined with an explicit expression but has to be compared against experiments [37]. Based on the results gathered [37], a value of 0.6 was used where it shows reasonable agreement with published experimental results. In order to balance between consumption of computational resources and numerical stability, the time step size was set to $1 \times 10^{-3}s$ as the solution has no issues with convergence using the established time step size (see section 3.2). Furthermore, the application of an initial condition for the gas phase aided in the numerical stability. This initial condition was

obtained by calculating a solution based only on the flow of a single gas phase and the solution was then used as the initial condition. A constant value of volume fraction was also applied throughout the entire domain before commencing two-phase simulations. From the experimental data, the particle mass concentration is mostly between 1 to $2kg/m^3$. Using the expression *particle mass concentration = volume fraction × particle density*, it was possible to deduce that the actual particle volume fraction within the pipe was in the order of 0.001. Consequentially, a value of 0.001 was used to patch the domain.

3. Numerical procedures

3.1 Mesh generation

When generating the mesh, a blocking strategy was applied. Across the stream wise cross-section, the pipe was divided into five blocks, one in the middle and four at the wall sides. At the bend, the geometry was sectioned into four parts over the whole 90°. Figure 1 shows an illustration of the blocking strategy at the bend. Such a blocking strategy allows the generation of a relatively uniform hexahedral mesh at the pipe bend. By utilizing hexahedral mesh at the pipe bend, it allows the majority of the computational cells to have its faces orientated perpendicular to the flow, hence, increasing the stability of the calculations. To address two-phase flows with numerical simulation, the size of the mesh should be much larger than the particle diameter and much smaller when compared to the system. Table 1 lists some of the previous two-phase flow studies who had published their mesh cells' data. For these authors, the volume of a single mesh cell falls within the order of 10^{-9} to $10^{-7}m^3$ regardless of either the Eulerian or Lagrangian method was used. With this mesh cell volume, both dense and dilute phase conveying had been satisfactorily computed. Hence, this study will attempt to utilize hexahedral meshes with cell volumes in the order of 10^{-9} to $10^{-7}m^3$. When the hexahedral mesh was generated from the blocks, the approximate dimensions

applied to the cells was $0.002 \times 0.002 \times 0.004m$. The longer dimension helped to reduce the total number of cells for the domain and was oriented stream wise. Figure 2 shows the hexahedral mesh that was generated. Statistics of the generated cells are provided in Table 2.

3.2 Convergence and mesh dependency

The convergence characteristics of the above-mentioned Eulerian scheme was first observed. To improve convergence behaviour, the volume fraction parameter was patched with a constant value throughout the domain. Together with the small time step applied, the convergence behaviour was exceptional. Figure 3 shows the scaled residuals of the continuity equations. Due to a large number of iterations, it was not possible to present the entire convergence behaviour. Nevertheless, part of it is shown here. Residual for the continuity equations was seen to rapidly decrease within the first few time steps and thereafter, increased a little to attain a rather constant value and steady behaviour. While the scaled residual did not go below the widely-practised value of 10^{-3}, it stayed within the same order of magnitude. Such display of consistency would be sufficient in a problem that advocates the application of minute time steps in the order of 10^{-7} to$10^{-5}s$ [41].

The outlet particle mass flow rate behaviour could be used to further ensure that the solution is satisfactory. Two other meshes, a coarser and a finer mesh, were also generated to perform a mesh dependency test. The problem was calculated in a transient state to obtain a pseudo-steady result. Figure 4 (left) shows the outlet particle mass flow rate over time. The spike in the outlet flow rate plot represents transient characteristics of the flow where accumulated particles during the start-up acceleration were ejected collectively when the flow approached pseudo-steady state. The particle output was seen to reach a steady value beyond two seconds of flow time. Hereafter, all data extracted were from $6s$ to $10s$ flow time and then

arithmetically averaged. Figure 4 (right) plots the air velocity across the pipe diameter at $0.1m$ after the bend. The coarser mesh presents a slight difference in the air velocity but the current mesh shows no discernible disagreement with that from the finer mesh. Hence, the current mesh sizing was deemed to be adequately small to achieve mesh independence and was selected to be used for subsequent calculations.

4. Results and discussion

4.1 Effects of different model constant for turbulent dispersion model

Here, the model constant of the turbulent dispersion model is varied and simulation results are presented in Figure 5. All other parameters remained constant. The figure emphasizes on the chosen model constant of 25 (solid black line) and experimental data (dashed black line). The results are compared with experimental data for air velocity and particle concentrations right after the bend. The left graph plots air velocity and the right is particle concentration, for different model constants as presented. While it seems that the model constant does not affect the air velocity drastically, there is a significant effect on the results of particle concentration. Indeed, the turbulent dispersion term is present only in the momentum equation of the solid phase. A change in particle volume fraction changes the flow behaviour of the gas phase. Therefore, with particle volume fractions in the order of 10^{-3}, the air velocity is not subject to drastic changes.

From the particle concentration plot, a model constant of $20 - 30$ presents reasonable match with experimental data. This is determined by a rough evaluation of the area under the curve through a trapezoidal method instead of comparing absolute values because the particle mass flux has to be taken into consideration. Or rather, roughly the same amount of material should flow through a given cross-sectional area in the experimental case and numerical simulations

and this can be obtained from a combination of particle concentration and particle velocity data. Hence, the model constant 15 is not considered even though its peak value coincides with experimental data because the area under the curve will then be significantly more than that of the experimental data. As the air velocity plots are the closest match when the turbulent dispersion model constant is 25, this value is being chosen for the model used in subsequent analysis. While numerical results associated with this value show certain discrepancies, they otherwise captured the flow characteristics adequately after the underlying causes of inaccuracies are considered.

4.2 Vertical pipe section

Figure 6 shows the plot of particle concentration in kg/m^3 at various sections of the vertical pipe section after the bend, as labelled. Dashed lines represent published experimental data and solid lines are the numerical simulation results, where they were all compared at the same physical locations used by the experimental study. The particle concentration is derived using the value of particle volume fraction and the material density of the glass beads ($= volume\ fraction \times 2500 kg/m^3$). At $y = 0.1$, 1.1 and $1.9m$, numerical simulations have a reasonable representation of the experimental case. The concern lies with $y = 0.6m$ where the match is rather incongruent. It is believed that the discrepancy might be due to a combination of factors. One of the postulated contributing factors is that the $y = 0.6m$ vicinity is where the concentrated particle rope (a region within the pipe cross-sectional area that more particles are concentrated) starts to disperse, thereby being a transitional zone that is inherently difficult to capture accurately. The peak distribution represents the particle rope and when the particles enter a pipe bend, inertial effects will tend to cluster the particles into a region of higher particle concentration. This area is usually located at the outer wall of the pipe bend. Furthermore, the curved pipe bend also generates a secondary flow in the form of

a pair of counter-rotating vortex pair that should aid in the dispersion of particle ropes. Together with the turbulent dispersion force, the secondary flow is expected to transport the particle rope towards the middle of the pipe and disperse it thereafter. Such a mechanism is postulated to be the cause behind the offset in the peak particle distribution from the walls (i.e. at $y = 0.1m$). Also, while the particle concentration plots differ, especially at $y = 0.6m$, the particle mass flux is consistent across other locations.

The numerical result is seen to have already dispersed a fraction of the particle rope at $y = 0.6m$ as compared to the experimental data. Such occurrence can appear when the cohesive nature of the particles is not taken into consideration. In numerical simulations, there are no cohesive forces between the particles, which allows them to disperse much easier and faster. As compared to the experimental case where cohesive forces between particles tend to agglomerate them into bigger lumps, thereby having more momentum to resist dispersion. Another possibility is that a vena-contracta is formed downstream of the pipe bend and leads to a low-pressure region, which might not have been accounted for in the present simulations. This is also evident from the $y = 1.9m$ plot, where the particles are more evenly distributed across the pipe cross-section as compared to experimental results. The exact causes for the above numerical discrepancies remain unknown at this point, though it is possible that they are due to the limitations in mesh refinement and/or FAD model.

Figure 7 is a plot of the velocity of air and particles arising from the present numerical simulations, together with experimental data for particle velocity, where they are compared at locations where the experimental data were taken. Note that an inconsistency can be discerned in the plot at $y = 0.1m$. Recall that the original experiments made use of particles that vary in particle diameter and comprise a considerable amount of very small particles

(<10μm). Such particles, will follow very closely to the air flow which results in particles being detected across the pipe cross-section (with non-zero air velocities), albeit at a very small concentration that might not be reflected in the particle concentration plot. In the current numerical simulations however, a constant particle diameter of $42\mu m$ is used, in which resulted in areas with no particles (as compared to very minute particles in the experiments). Hence, the numerical model predicted zero particle velocity in areas where there are no particles present. As with the particle concentration, $y = 0.6m$ for particle velocity presents a little deviation from the experimental data and the reasons could be attributed to disregarding the effects of cohesiveness as detailed above. $y = 1.1$ and $1.9m$ plots present a reasonable match. For $y = 0.6$, 1.1 and $1.9m$, the air and particles' velocity differs only a little from each other. This is because the Stokes number, a measure of the responsiveness of the particle to the changes in its carrier gas, of the $42\mu m$ particle in this flow is small. Hence, the particle follows the air closely albeit with a small slip velocity present [42].

For completeness, the RMS velocity is plotted in Figure 8. In the published study, RMS velocity fluctuation of particles in the axial direction was measured. However, in the numerical simulation, only the turbulent kinetic energy (k) values of the air-particle mixture is available. The RMS velocity fluctuations are therefore obtained by $u' = \sqrt{2k/3}$. This expression assumes the velocity fluctuations to be isotropic and the resulting graphs show a lower absolute value than that measured in the experiments. This suggests that the velocity fluctuations are anisotropic with dominance in the stream wise direction. While the model under-predicts the velocity fluctuations, the agreement is still acceptable in terms of the trends. As the numerical model did not take into account different particle sizes, the particle size distribution plots will not be discussed here.

4.3 Horizontal pipe section

Figure 9 top row plots the particle concentration distribution in the horizontal pipe section at various locations as indicated by z, where the z locations are measured from the pipe inlet. For $z = 2.5$ and $4.5m$, the plots are superimposed on the same graph. The disagreement between simulation results and experimental data is substantial. In the experiments, the bulk of the particles are seen to concentrate at the bottom of the pipe. However, it seems that the particles are fairly evenly distributed in the simulation results and does not move towards the bottom of the pipe as seen in the experiments. This is the same issue that some previous studies had reported. For instance, Hidayat and Rasmuson [13] had a similar issue where their numerical results did not represent the experimental data in a horizontal pipe section. They had attributed this to the misinterpretation of experimental data by the original researchers and used the concept of particle terminal velocity to support their claim. They utilized the terminal velocity of a particle in free fall to calculate the time it would take for the particle to travel from the top to the bottom of the pipe. Subsequently, they used the absolute particle axial velocity to calculate how far would the particle travel downstream during this period of time before reaching the bottom of the pipe. They concluded that the particle should reach the bottom of the pipe twenty times further downstream as compared to the experiments, which represents a significant discrepancy.

However, it should be noted that they had neglected the downward-acting velocity induced by the secondary flows of the carrier gas, which will hasten the movement of the particles towards the bottom of the pipe further. Including this velocity component in the analysis will provide a more accurate assessment of the flow scenario. Another plausible contributing factor could be due to the exclusion of the particle diameter variations during the numerical

simulations and results presented in Section 4.4 appear to support this claim. While the model prediction differs from the experimental data, it can be seen that the particle concentration distributions do not differ much between these two locations ($z = 2.5$ and $4.5m$) in both experimental and numerical results. Therefore, the results are consistent, even though good accuracy has not been achieved in the current simulation.

For the particle velocity plots shown in Figure 9 middle row, only the $z = 0.5m$ location display a discrepancy to experimental data which suggests a possibly undeveloped velocity profile for the simulation. This is because, in the experiment, $z = 0m$ is the last honeycomb which was used to ensure even distribution of particles. These honeycomb structures might not have produced its intended function perfectly, contributing to the mismatch in numerical results and experimental data at both the particle concentration distribution and particle velocity plots. The RMS velocity fluctuations are shown in Figure 9 bottom row and are derived from the same expression used in the vertical pipe section. Like the particle velocity plots, numerical results at $z = 2.5$ and $4.5m$ shows a decent match to experimental data. Again, $z = 0.5m$ does not match well for the same reason stated earlier. The honeycomb structures are believed to have induced additional turbulence in the flow, hence, the higher velocity fluctuations as presented in the experimental data.

4.4 Effects of particle diameter

Considering the sizable difference between numerical results and experimental data for the particle concentration present within the horizontal pipe section, a potential cause is with the numerical model not taking into consideration the particle diameter. Firstly, particle diameter variations will be present in practical applications of material transported by pneumatic conveying. Such variations are accounted for in the experiments but not in the current

numerical work. Secondly, the multitude of some other factors will contribute to variations in the actual particle diameter present within the pipeline. Such factors include the effects of humidity, cohesiveness of the material or electrostatic forces that may contribute to agglomeration of the particles, resulting in effectively larger particle diameters. For that reason, the simulation was run with a particle diameter of $100\mu m$ (as compared to the initial $42\mu m$) to simulate the presence of larger diameter particles within the conveying process. Figure 10 graphs the results of assuming larger particle diameter in the horizontal pipe section. Here, it shows that inertial and gravitation forces come into greater effect with increasing particle diameter resulting in the concentration of particles increasing near the bottom of the pipe.

From this, it can be seen that once the variation of particle diameter is taken into consideration, the precision of the numerical model increases dramatically even though the approach taken here is just a simple increment in the particle diameter. To improve prediction of the flow characteristics, it is possible to define multiple 'Eulerian' phases for the solids phase using different particle diameters, based on the actual distribution, for each 'Eulerian' phase defined. However, care has to be taken when utilizing this method as each additional phase introduces its individual set of conservation equations and might prove to be computationally expensive in applications of large domain sizes. Also, defining more phases for different particle diameters still does not account for agglomeration effects. To integrate the effect of particle diameter variations due to other factors (humidity, cohesiveness of the material or electrostatic forces) within a single numerical model, it will require relations that deal with coalescence and break-up of the particles. These are very specific situations that may even touch on the chemistry of the individual particles itself and is, therefore, out of the scope of the current study.

Nevertheless, these problems are being tackled by researchers. Korevaar et al. [43] and Pei et al. [44] for example, used the Lagrangian scheme with appropriate modelling to investigate contact electrification effects of particles. Experimental investigations on electrostatic effects were also performed by Yao et al. [45]. Humidity and effects from particle properties were also covered by Karde and Ghoroi [46] and Shah et al. [47] respectively. These examples serve as a starting point for future works proposing to incorporate such effects into the Eulerian granular model.

5. Conclusions

The application of a multiphase numerical model with Eulerian treatment for the solid phase is presented here, where validation of the model is mainly based on previously published experimental results. In applying the FAD turbulent dispersion model, its model constant is varied to determine the most appropriate value for dilute flows. The model constant is observed to have a greater effect on the particle concentration distribution than on the gas phase velocity, and a most appropriate model constant was selected for to compare with earlier experimental results. Note that while numerical results show certain discrepancies, they otherwise captured the flow characteristics adequately after addressing the underlying cause of inaccuracies.

Gas-phase velocity is well predicted for both vertical and horizontal pipe sections. However, the accuracy of the model in predicting particle concentration distribution is a little less satisfactory in certain areas of the pipe. In the vertical pipe section, the inaccuracy results from the difficulty of capturing the transitional zone where the particle rope starts to disperse. Outside this dispersion zone, the model was able to predict the particle concentration adequately. For the horizontal pipe section, initially, it appears that the model is grossly erroneous in predicting particle concentrations. However, particle diameter variations appear

to account for the mismatch. The simulation is repeated with an increased particle diameter and the model is then able to capture the experimental particle concentration distribution in the horizontal pipe section with noticeable accuracy, which demonstrated the suitability of employing the Eulerian treatment for two-phase gas-particle flows.

Nomenclature

C_{TD}	Turbulent dispersion constant
d_s	Particle diameter
D_s	Dispersion scalar
e_{ss}	Coefficient of restitution
F_{td}	Turbulent dispersion force
g	Acceleration due to gravity
$g_{0,ss}$	Radial distribution function
$\bar{\bar{I}}$	Identity tensor
k_{Θ_s}	Diffusion coefficient
K_{pq}	Interphase momentum exchange coefficient
p	Pressure
R_{pq}	Interaction term between phase p and q
Re	Relative Reynolds number
t	Time
v	Velocity
α	Volume fraction
γ_{Θ_s}	Collisional dissipation of energy
Θ_s	Granular temperature

λ	Bulk viscosity
μ	Shear viscosity
ρ	Density
σ	Turbulent Prandtl number
τ	Stress tensor
ϕ	Internal angle of friction

Acknowledgements

The authors gratefully acknowledge the support for the research by Maritime and Port Authority of Singapore and Jurong Port Pte Ltd under a MPA-JP MINT Fund grant (TRIDENT 003-12-068), Nanyang Technological University High Performance Computing Centre, and University of Southampton IRIDIS High Performance Computing Facility.

References

[1] D. Mills, Pneumatic conveying design guide: Butterworth-Heinemann, 2003.

[2] C. T. Crowe, Multiphase flow handbook: CRC press, 2014.

[3] W. C. Yang, Handbook of fluidization and fluid-particle systems: CRC press, 2003.

[4] G. E. Klinzing, Pneumatic conveying of solids: A theoretical and practical approach: Springer, 1997.

[5] T. S. Khan, Y. Dai, M. S. Alshehhi, and L. Khezzar, "Experimental flow characterization of sand particles for pneumatic transport in horizontal circular pipes," *Powder Technology*, 2016.

[6] M. S. de Moraes et al., "Experimental quantification of the head loss coefficient K for fittings and semi-industrial pipe cross section solid concentration profile in pneumatic

conveying of polypropylene pellets in dilute phase," *Powder Technology*, vol. 310, pp. 250-263, 2017.

[7] A. Adeniji-Fashola and C. Chen, "Modeling of confined turbulent fluid-particle flows using Eulerian and Lagrangian schemes," *International Journal of Heat and Mass Transfer*, vol. 33, pp. 691-701, 1990.

[8] B. Vreman, B. J. Geurts, N. Deen, J. Kuipers, and J. Kuerten, "Two-and four-way coupled Euler–Lagrangian large-eddy simulation of turbulent particle-laden channel flow," *Flow, Turbulence and Combustion*, vol. 82, pp. 47-71, 2009.

[9] S. Elghobashi, "On predicting particle-laden turbulent flows," *Applied Scientific Research*, vol. 52, no. 4, pp. 309-329, 1994.

[10] D. McGlinchey, A. Cowell, E. Knight, J. Pugh, A. Mason, and B. Foster, "Bend pressure drop predictions using the Euler-Euler model in dense phase pneumatic conveying," *Particulate Science and Technology*, vol. 25, pp. 495-506, 2007.

[11] A. B. Makwana, A. Patankar, and M. Bose, "Effect of Dune Formation on Pressure Drop in Horizontal Pneumatic Conveying System," *Particulate Science and Technology*, vol. 33, pp. 59-66, 2015.

[12] J. Li, C. Webb, S. Pandiella, G. M. Campbell, T. Dyakowski, A. Cowell, et al., "Solids deposition in low-velocity slug flow pneumatic conveying," *Chemical Engineering and Processing: Process Intensification*, vol. 44, pp. 167-173, 2005.

[13] M. Hidayat and A. Rasmuson, "Some aspects on gas–solid flow in a U-bend: numerical investigation," *Powder Technology*, vol. 153, pp. 1-13, 2005.

[14] D. McGlinchey, A. Cowell, and R. Crowe, "CFD investigation of dense phase pneumatic conveying at a pipeline enlargement," *Particuology*, vol. 10, pp. 176-183, 2012.

[15] N. Behera, V. K. Agarwal, M. G. Jones, and K. C. Williams, "CFD modeling and analysis of dense phase pneumatic conveying of fine particles including particle size distribution," *Powder Technology*, vol. 244, pp. 30-37, 2013.

[16] K. Ibrahim, M. El-Kadi, M. Hamed, and S. M. El-Behery, "Effect of bend orientation and flow direction on the behaviour of gas–solid flow," in *Proceedings 8th International Conference of Fluid Dynamics and Propulsion*, 2006, pp. 14-17.

[17] R. Schallert and E. Levy, "Effect of a combination of two elbows on particle roping in pneumatic conveying," *Powder Technology*, vol. 107, pp. 226-233, 2000.

[18] N. Huber and M. Sommerfeld, "Modelling and numerical calculation of dilute-phase pneumatic conveying in pipe systems," *Powder Technology*, vol. 99, pp. 90-101, 1998.

[19] W. Pu, C. Zhao, Y. Xiong, C. Liang, X. Chen, P. Lu, et al., "Numerical simulation on dense phase pneumatic conveying of pulverized coal in horizontal pipe at high pressure," *Chemical Engineering Science*, vol. 65, pp. 2500-2512, 2010.

[20] J. t. van Deemter and E. van der Laan, "Momentum and energy balances for dispersed two-phase flow," *Applied Scientific Research*, vol. 10, pp. 102-108, 1961.

[21] T. B. Anderson and R. Jackson, "A fluid mechanical description of fluidized beds. Equations of motion," *Industrial & Engineering Chemistry Fundamentals*, vol. 6, pp. 527-539, 1967.

[22] S. Ergun, "Fluid flow through packed columns," *Chemical Engineering Progress*, vol. 48, pp. 89-94, 1952.

[23] C. Wen and Y. Yu, "Mechanics of fluidization," in *Chemical Engineering Progress Symposium Series*, 1966, pp. 100-101.

[24] D. Gidaspow, Multiphase flow and fluidization: continuum and kinetic theory descriptions: Academic press, 1994.

[25] J. Ding and D. Gidaspow, "A bubbling fluidization model using kinetic theory of granular flow," *American Institute of Chemical Engineers Journal*, vol. 36, pp. 523-538, 1990.

[26] C. Lun, S. B. Savage, D. Jeffrey, and N. Chepurniy, "Kinetic theories for granular flow: inelastic particles in Couette flow and slightly inelastic particles in a general flowfield," *Journal of Fluid Mechanics*, vol. 140, pp. 223-256, 1984.

[27] S. Lee and F. Durst, "On the motion of particles in turbulent duct flows," *International Journal of Multiphase Flow*, vol. 8, pp. 125-146, 1982.

[28] D. Modarress, S. Elghobashi, and H. Tan, "Two-component LDA measurement in a two-phase turbulent jet," *American Institute of Aeronautics and Astronautics Journal*, vol. 22, pp. 624-630, 1984.

[29] Y. Tsuji, Y. Morikawa, and H. Shiomi, "LDV measurements of an air-solid two-phase flow in a vertical pipe," *Journal of Fluid Mechanics*, vol. 139, pp. 417-434, 1984.

[30] A. D. Burns, T. Frank, I. Hamill, and J.-M. Shi, "The Favre averaged drag model for turbulent dispersion in Eulerian multi-phase flows," in *5th International Conference on Multiphase Flow*, 2004, pp. 1-17.

[31] B. van Wachem, J. Schouten, C. van den Bleek, R. Krishna, and J. Sinclair, "Comparative analysis of CFD models of dense gas-solid systems," *American Institute of Chemical Engineers Journal*, vol. 47, pp. 1035-1051, 2001.

[32] M. Syamlal, W. Rogers, and T. J. O'Brien, "MFIX documentation: Theory guide," *National Energy Technology Laboratory, Department of Energy, Technical Note*, 1993.

[33] D. Gidaspow, R. Bezburuah, and J. Ding, "Hydrodynamics of circulating fluidized beds: kinetic theory approach," Illinois Institute of Technology, Chicago, IL (United States). Department of Chemical Engineering, 1991.

[34] P. C. Johnson and R. Jackson, "Frictional–collisional constitutive relations for granular materials, with application to plane shearing," *Journal of Fluid Mechanics*, vol. 176, pp. 67-93, 1987.

[35] N. Huber and M. Sommerfeld, "Characterization of the cross-sectional particle concentration distribution in pneumatic conveying systems," *Powder Technology*, vol. 79, pp. 191-210, 1994.

[36] T. Li and S. Benyahia, "Revisiting Johnson and Jackson boundary conditions for granular flows," *American Institute of Chemical Engineers Journal*, vol. 58, no. 7, pp. 2058-2068, 2012.

[37] C. Loha, H. Chattopadhyay, and P. K. Chatterjee, "Euler-Euler CFD modeling of fluidized bed: Influence of specularity coefficient on hydrodynamic behavior," *Particuology*, vol. 11, no. 6, pp. 673-680, 2013.

[38] T. Y. Quek, C.-H. Wang, and M. B. Ray, "Dilute gas-solid flows in horizontal and vertical bends," *Industrial & engineering chemistry research*, vol. 44, pp. 2301-2315, 2005.

[39] K. Chu and A. Yu, "Numerical simulation of the gas− solid flow in three-dimensional pneumatic conveying bends," *Industrial and Engineering Chemistry Research*, vol. 47, pp. 7058-7071, 2008.

[40] S. Laín and M. Sommerfeld, "Characterisation of pneumatic conveying systems using the Euler/Lagrange approach," *Powder Technology*, vol. 235, pp. 764-782, 2013.

[41] H. Li and S. A. Vasquez, "Numerical simulation of steady and unsteady compressible multiphase flows," in *ASME 2012 International Mechanical Engineering Congress and Exposition*, 2012, pp. 2239-2251.

[42] W. C. Hinds, "Aerosol technology: properties, behavior, and measurement of airborne particles," *New York, Wiley-Interscience*, 1982. 442 p., vol. 1, 1982.

[43] M. Korevaar, J. Padding, M. A. Van der Hoef, and J. Kuipers, "Integrated DEM–CFD modeling of the contact charging of pneumatically conveyed powders," *Powder Technology*, vol. 258, pp. 144-156, 2014.

[44] C. Pei, C. Y. Wu, D. England, S. Byard, H. Berchtold, and M. Adams, "Numerical analysis of contact electrification using DEM–CFD," *Powder Technology*, vol. 248, pp. 34-43, 2013.

[45] J. Yao *et al.*, "Experimental investigations of granular shape effects on the generation of electrostatic charge," *Particuology*, vol. 15, pp. 82-89, 2014.

[46] V. Karde and C. Ghoroi, "Fine powder flow under humid environmental conditions from the perspective of surface energy," *International Journal of Pharmaceutics*, vol. 485, no. 1, pp. 192-201, 2015.

[47] U. V. Shah, V. Karde, C. Ghoroi, and J. Y. Heng, "Influence of particle properties on powder bulk behaviour and processability," *International Journal of Pharmaceutics*, vol. 518, no. 1-2, pp. 138-154, 2017.

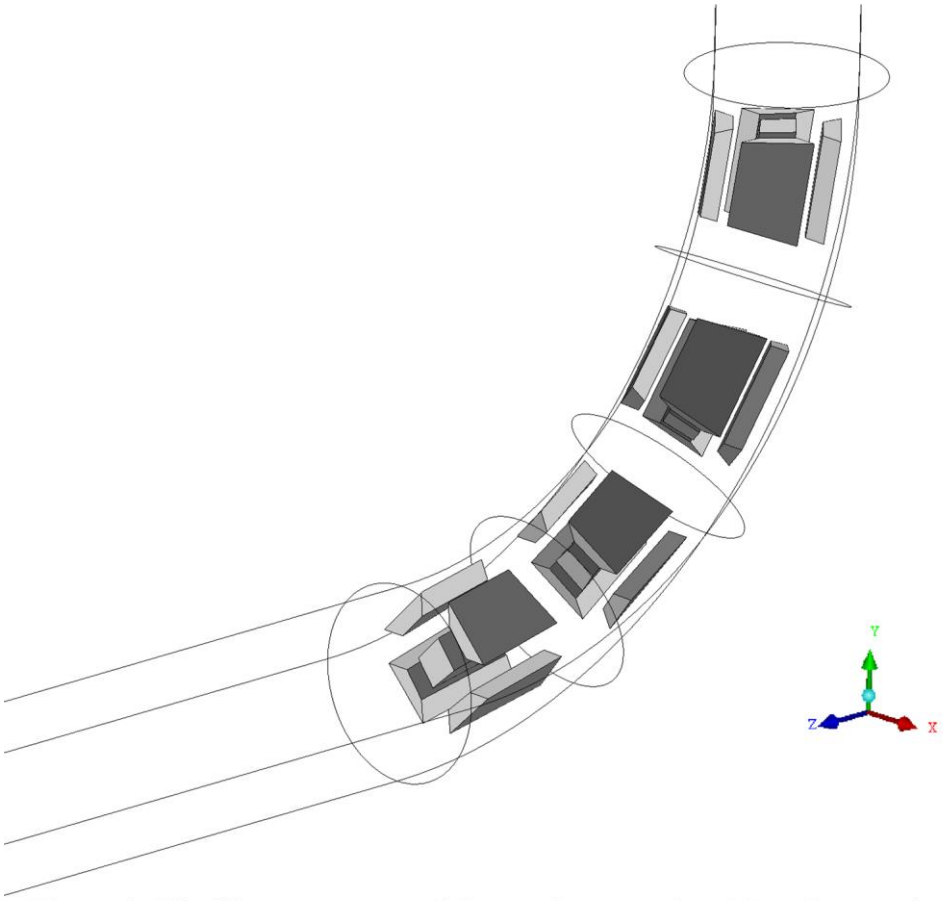

Figure 1 Blocking strategy used for mesh generation. Note that gravity acts in the negative y-direction.

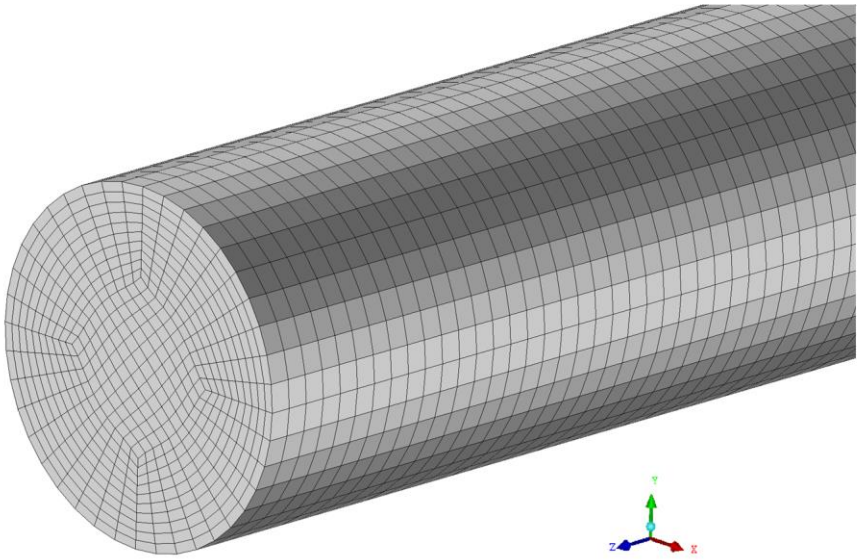

Figure 2 Hexahedral mesh generated, cell volume ranges in the order of 10^{-9} to $10^{-7}m^3$

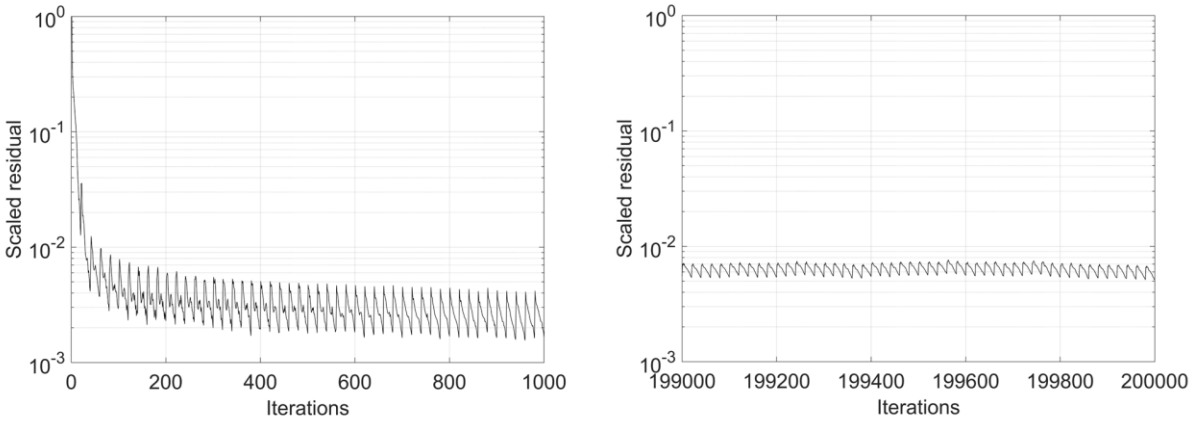

Figure 3 Scaled residual for the continuity equations

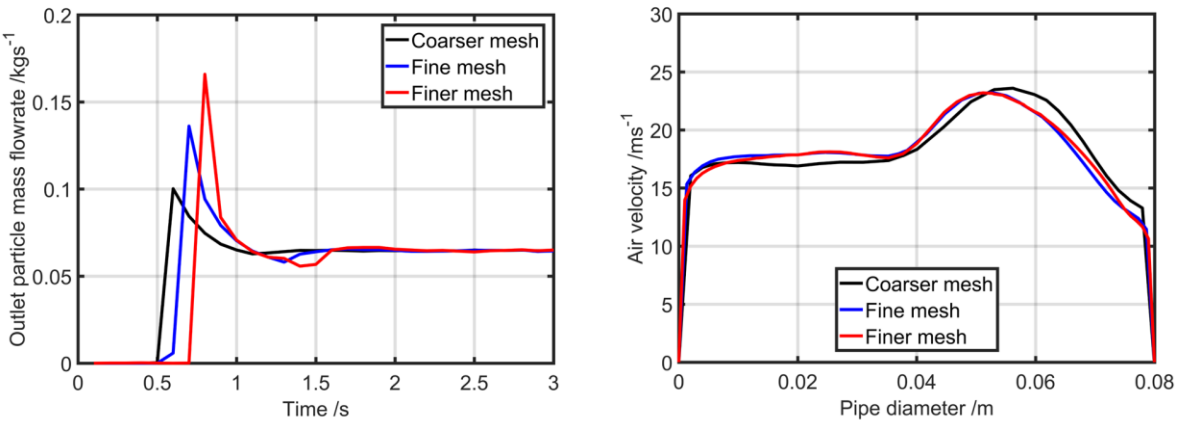

Figure 4 Outlet particle mass flowrate (left) and air velocity plot at 0.1m after the bend (right)

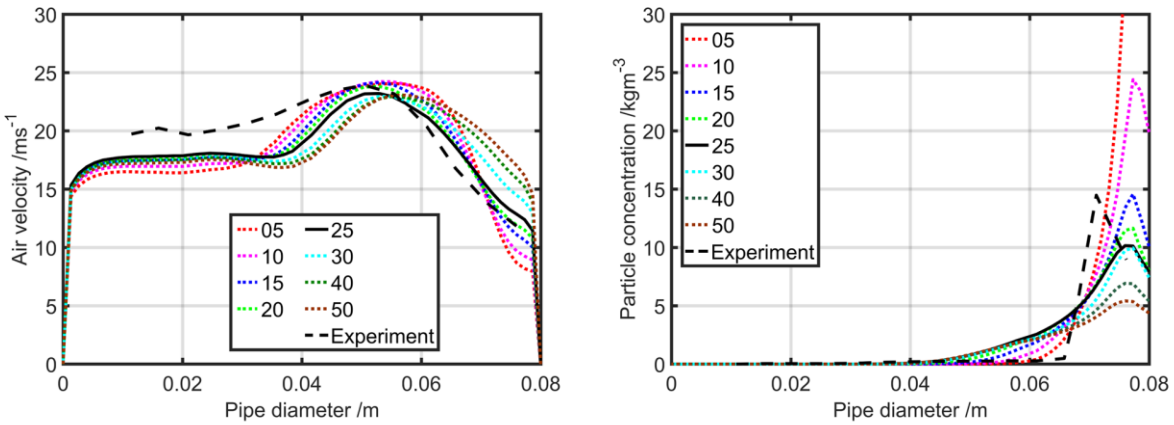

Figure 5 Effects of different model constant for turbulent dispersion model on air velocity (left) and particle concentration (right). The model constant refers to C_{TD} used in Equation 9.

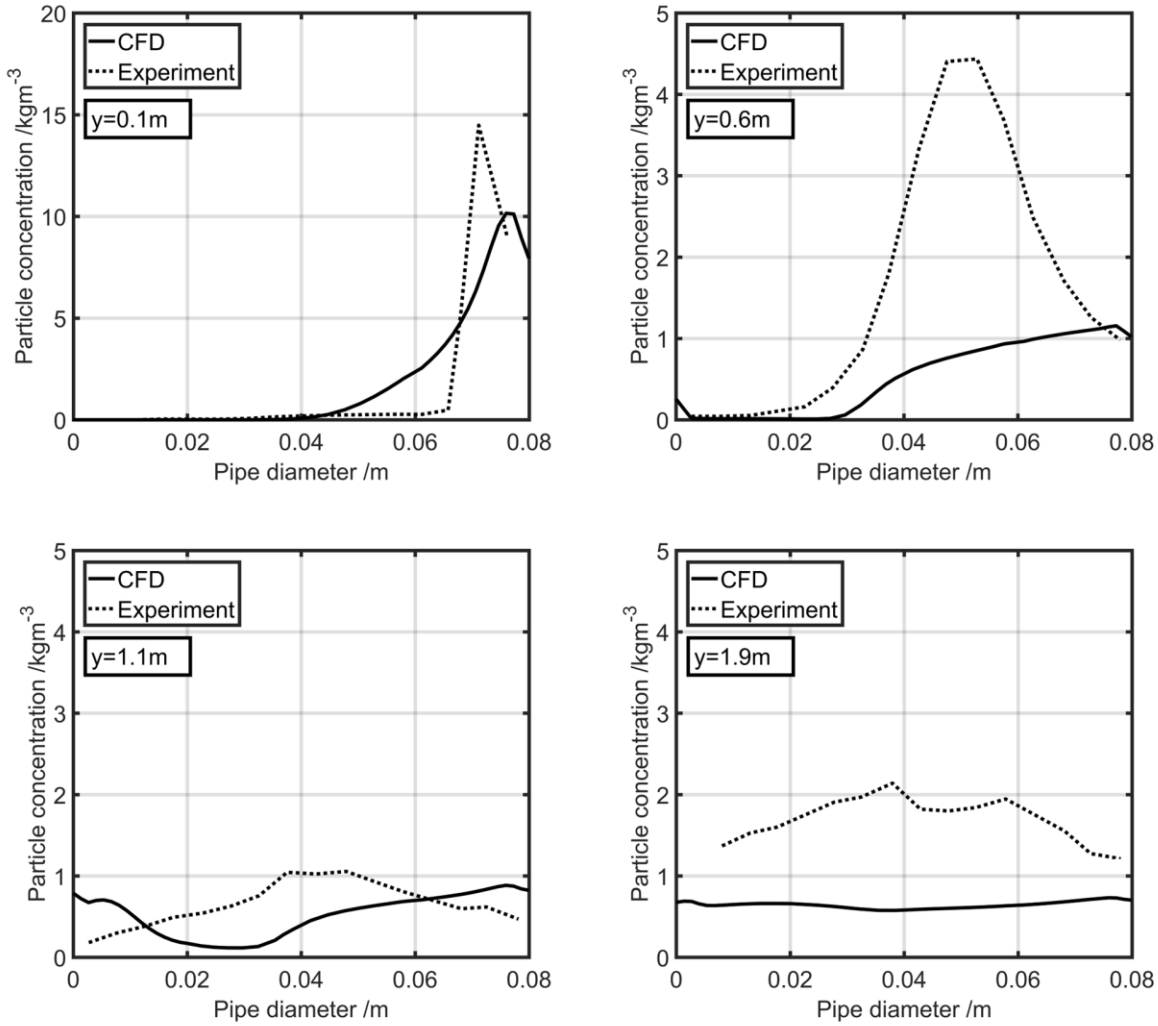

Figure 6 Comparison of CFD results with experimental data of particle concentration along various vertical sections after the pipe bend as indicated

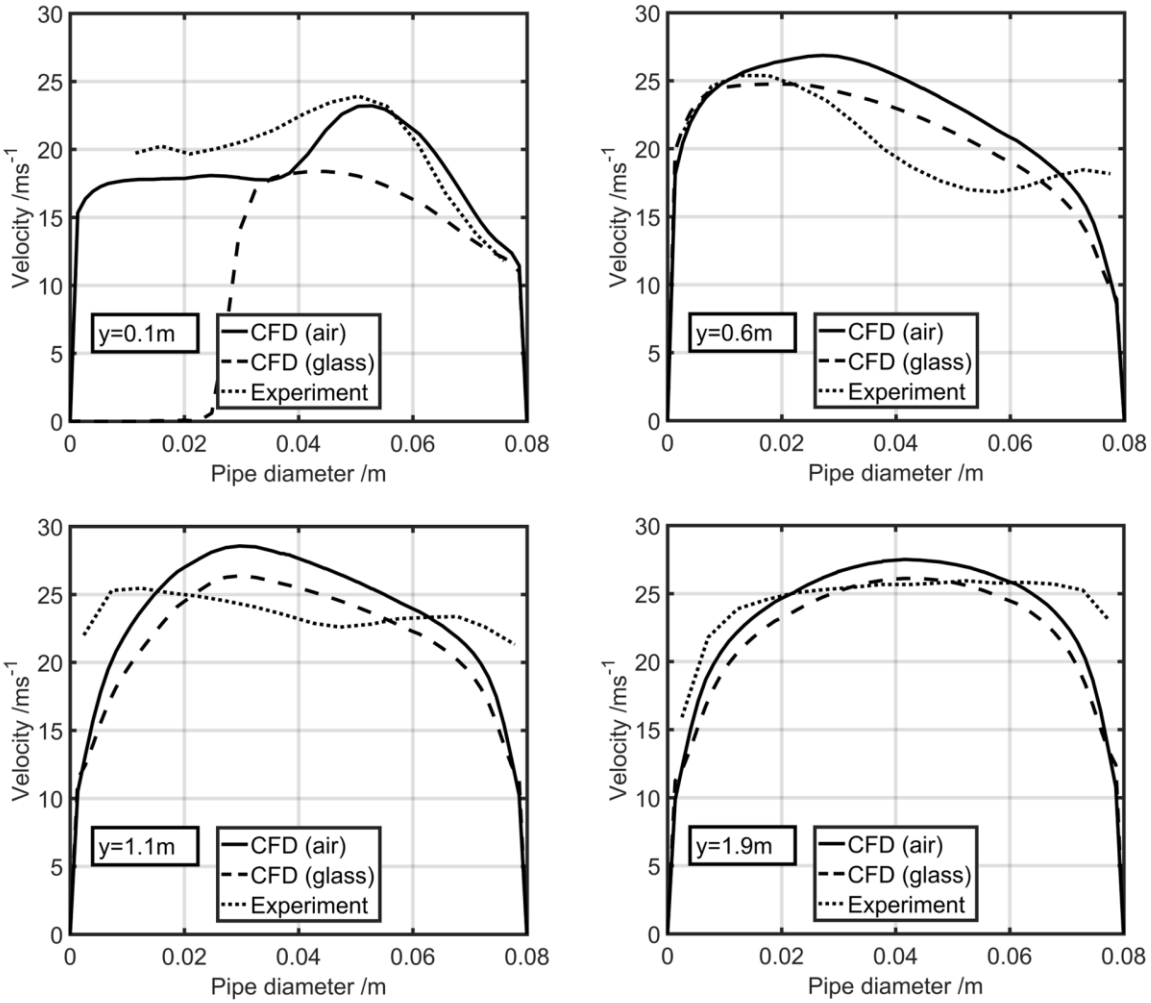

Figure 7 Comparison of CFD results with experimental data of particle velocity along various vertical sections after the pipe bend as indicated

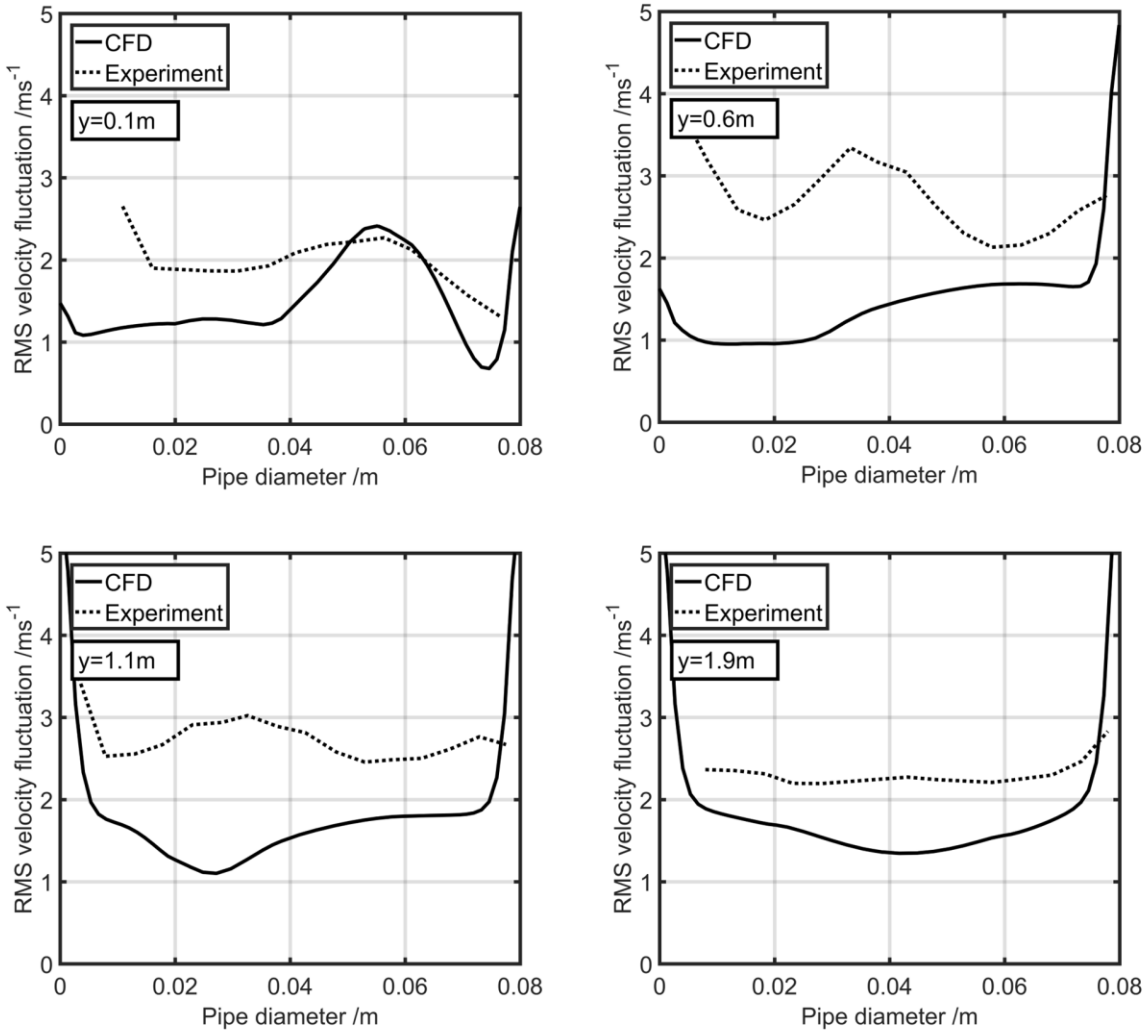

Figure 8 Comparison of CFD results with experimental data of RMS particle fluctuation along various vertical sections after the pipe bend as indicated

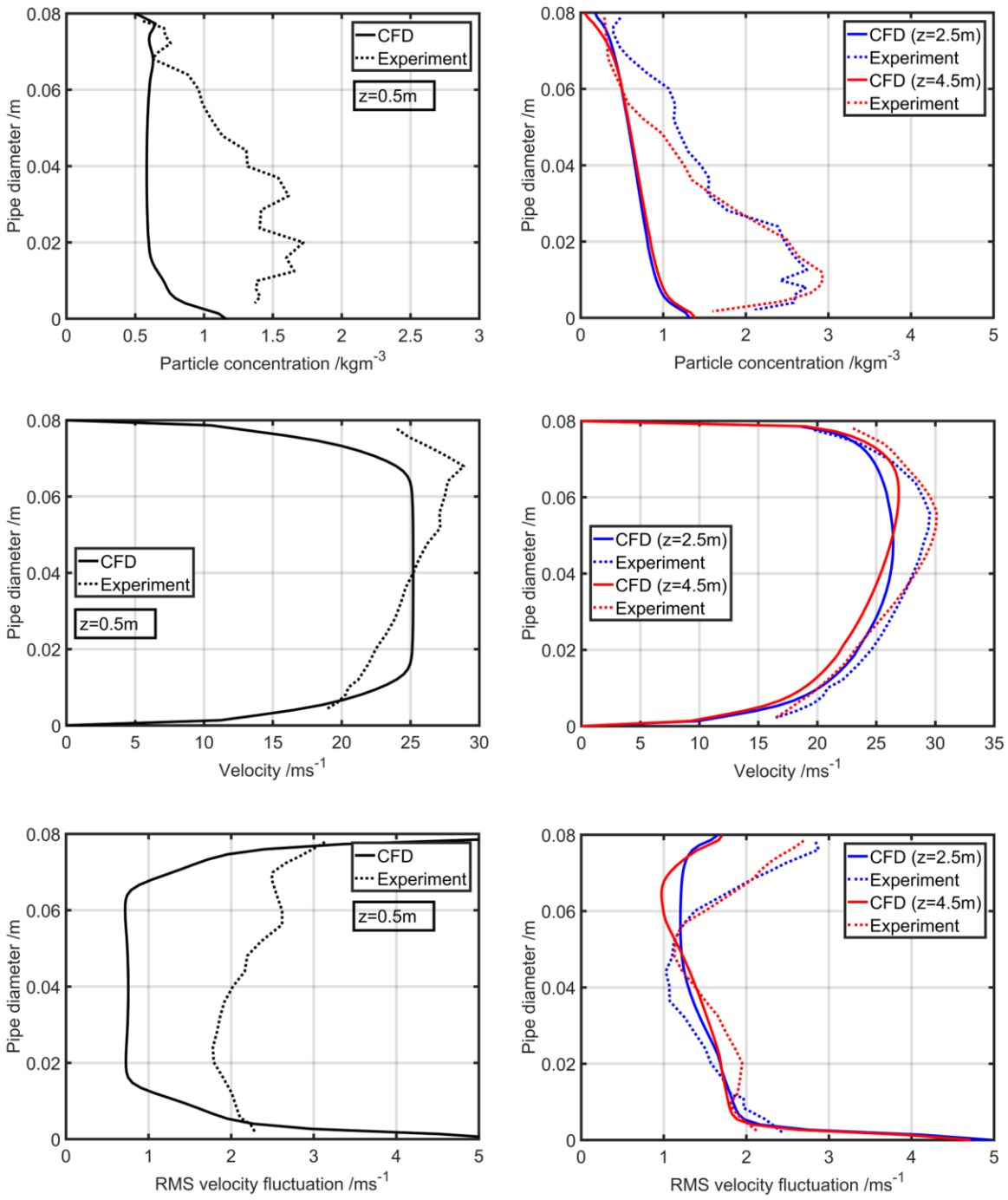

Figure 9 Comparison of CFD results with experimental data of particle concentration (top row), air velocity (middle row) and RMS velocity fluctuation (bottom row) along various horizontal sections before the pipe bend as indicated. Note that z values are measured from the pipe inlet.

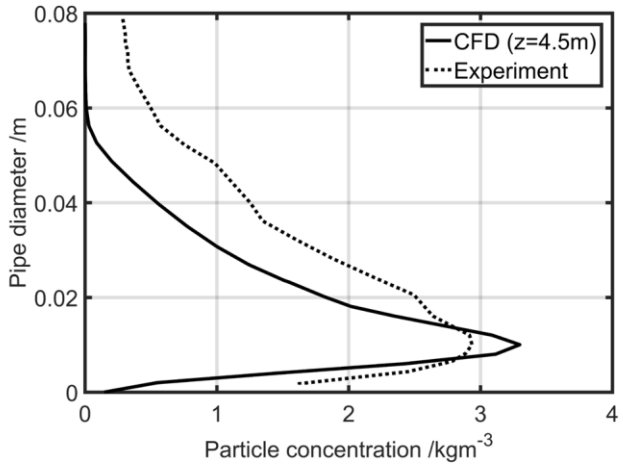

Figure 10 Particle concentration distribution within the horizontal pipe section when particle diameter increased to 100μm

Table 1 List of studies and their reported mesh sizes

Study	Type	Volume of elements $/m^3$
Quek, Wang, and Ray [38]	Lagrangian study of dilute flow	8.67×10^{-9} to 1.37×10^{-7}
Behera, Agarwal, Jones, and Williams [15]	Eulerian study of dense flow	3.83×10^{-8} to 1.26×10^{-7}
Chu and Yu [39]	Lagrangian study of dilute flow	3.51×10^{-8} to 6.17×10^{-7}
Laín and Sommerfeld [40]	Lagrangian study of dilute flow	avg. 3.18×10^{-7}

Table 2 Cell statistics

Number of cells	2976750
Min. volume	5.426e-9
Max. volume	3.210e-8
Min. orthogonal quality	0.706
Max. orthogonal skew	0.294
Max. aspect ratio	5.210

Graphical abstract

An Eulerian granular numerical model was applied to a horizontal-to-vertical pneumatic conveying pipe to study the effects of turbulent dispersion force on particles. Model inaccuracies were accounted for.

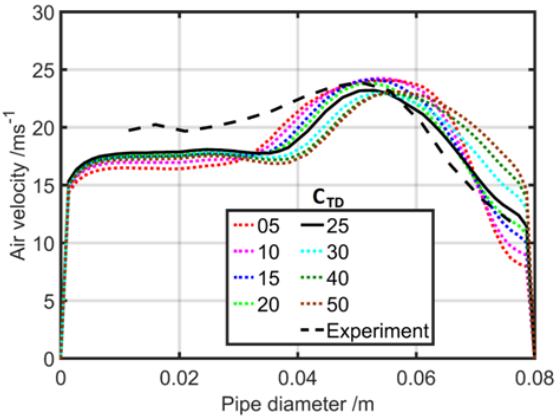

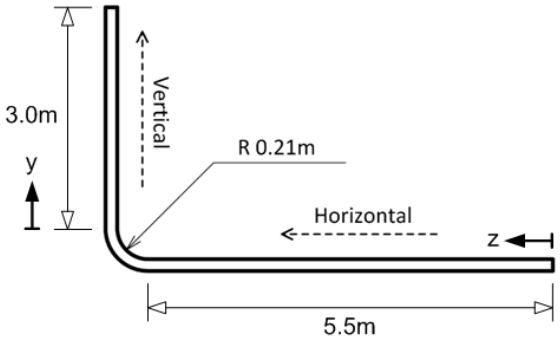

(a) Turbulent dispersion model constant effects on conveying air velocity in the vertical pipe

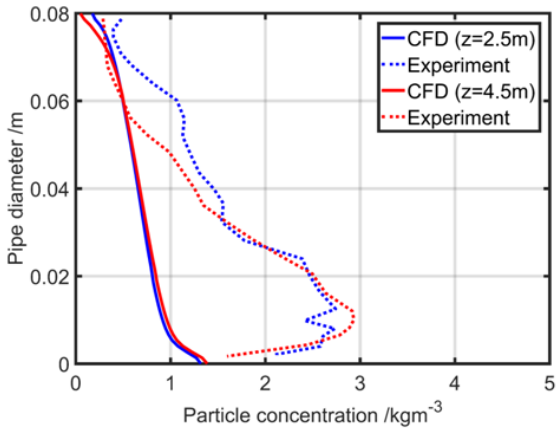

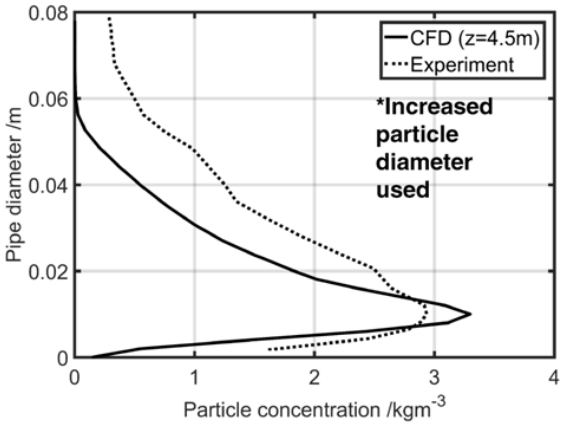

(b) Particle diameter accounts for inaccuracies in numerical simulation. Increasing particle diameter greatly improved simulation accuracy in the horizontal pipe section

Highlights

- An Eulerian granular model has been validated against experimental results.
- Application of Favre Averaged Drag model towards gas-solid flows is appropriate.
- Neglecting particle agglomeration effects causes inaccuracies in simulations.
- Good consistency displayed by the numerical model in predicting gas-solid flows.